# Comparing the Longwave Effective Cloud Fraction to Cloudiness Measurements

*E. E. Takara and R. G. Ellingson*
*Department of Meteorology*
*Florida State University*
*Tallahassee, Florida*

## Introduction

The Cloudiness Intercomparison intensive operational period (IOP) took place from February through May 2003 at the southern great plains (SGP) Central Facility. Its purpose was to compare several different instruments and methods of measuring cloud amount. In this extended abstract, the longwave effective cloud fraction ($N_e$) is described and compared to cloudiness measurements from the Total Sky Imager (TSI).

F, the average longwave surface over a large area can be expressed using $N_e$ as:

$$F = (1 - N_e)F_{clear} + N_e F_{overcast} \qquad (1)$$

$F_{clear}$ is the clear sky flux; the flux that would occur if the broken cloud field was removed. $F_{overcast}$ is the flux that would occur if the broken cloud field became completely overcast. $N_e$ is the fractional sky coverage of flat black plates.

## Instruments and Measurements

Rearranging (1) to solve for $N_e$ yields:

$$N_e = \frac{F - F_{clear}}{F_{overcast} - F_{clear}} \qquad (2)$$

In Han and Ellingson (1999) longwave parameterizations were found for cumulus cloud fields. In that study, F, $F_{clear}$, and $F_{overcast}$ were obtained through measurements, fixing $N_e$. That process is used here for all skies.

Several data sets from the Atmospheric Radiation Measure (ARM) SGP central facility were used to derive $N_e$. The Atmospheric Emitted Radiance Interferometer (AERI) radiances and surface emitting temperature along with the Active Remote Sensing of Cloud Layers (ARSCL) cloud base were used to derive the $F_{clear}$, and $F_{overcast}$ throughout the day. This resulted in continuous envelopes of clear and

overcast fluxes. The longwave ($0-3000\text{cm}^{-1}$) downward flux, F, was measured directly by pyrgeometer. The Total Sky Imager (TSI) opaque hemispherical cloud amount was used for comparison.

## Computing $F_{clear}$ and $F_{overcast}$

Assuming that the downwelling radiance outside the $833-1250\text{ cm}^{-1}$ window can be approximated by the Planck function ($B_\nu$), a pseudo-window radiance ($I_w$) can be defined as:

$$I_{AERI}^{tot} = \sum I_{AERI} \tag{3}$$

$$I_w = I_{AERI}^{tot} - \int_{520\text{cm}^{-1}}^{833\text{cm}^{-1}} B_\nu(T_{surf}, \nu)d\nu - \int_{1250\text{cm}^{-1}}^{3020\text{cm}^{-1}} B_\nu(T_{surf}, \nu)d\nu \tag{4}$$

The combination of a low standard deviation in the AERI measured $990\text{cm}^{-1}$ radiance and a high $I_w$ indicates the presence of clouds; a low standard deviation and low $I_w$ indicates clear skies. The threshold values of $I_w$ change according to the surface temperature and water vapor amounts.

The clear and overcast fluxes can be computed from the $I_w$ according to:

$$I_{AERI}^{tot} = I_w + \int_{520\text{cm}^{-1}}^{833\text{cm}^{-1}} B_\nu(T_{surf}, \nu)d\nu + \int_{1250\text{cm}^{-1}}^{3020\text{cm}^{-1}} B_\nu(T_{surf}, \nu)d\nu \tag{5}$$

$$F_{clear/overcast} = LI_{AERI}^{tot} + \pi \int_{0\text{cm}^{-1}}^{520\text{cm}^{-1}} B_\nu(T_{surf}, \nu)d\nu + \delta_{pyr-AERI} \tag{6}$$

Where L is a conversion factor ranging from $\pi$ at the surface to 2.45 for clear skies and $\delta_{pyr-AERI}$ is an instrument offset. By iteration, known clear and overcast can be found and used to construct the clear and overcast flux envelopes throughout the day. The flux envelopes can be used to find $N_e$.

## Comparing $N_e$

Figure 1 is a scatter plot of the opaque TSI cloud amount and the derived $N_e$ for times where the lowest ARSCL cloud base ($Z_b$) was less than 4km; it also includes all clear sky cases. The derived $N_e$ underestimates the cloud amount in most cases. While there is a great deal of scatter, there is some agreement; with significant clustering for clear ($N_e=0$) and overcast ($N_e=1$). The dots circled in red show where the $N_e$ algorithm had difficulty recognizing deviations from completely clear and overcast conditions.

Figure 2 is a scatter plot of the opaque TSI cloud amount and the derived $N_e$ for times where the $Z_b$ was greater than or equal to 4 km but less than 8 km. Again, the derived $N_e$ consistently underestimated the

cloud amount. The scatter is similar to the plot for Zb < 4 km, with slightly more departure from the 1:1 line. The dots circled in red indicate a problem with detecting higher clouds.
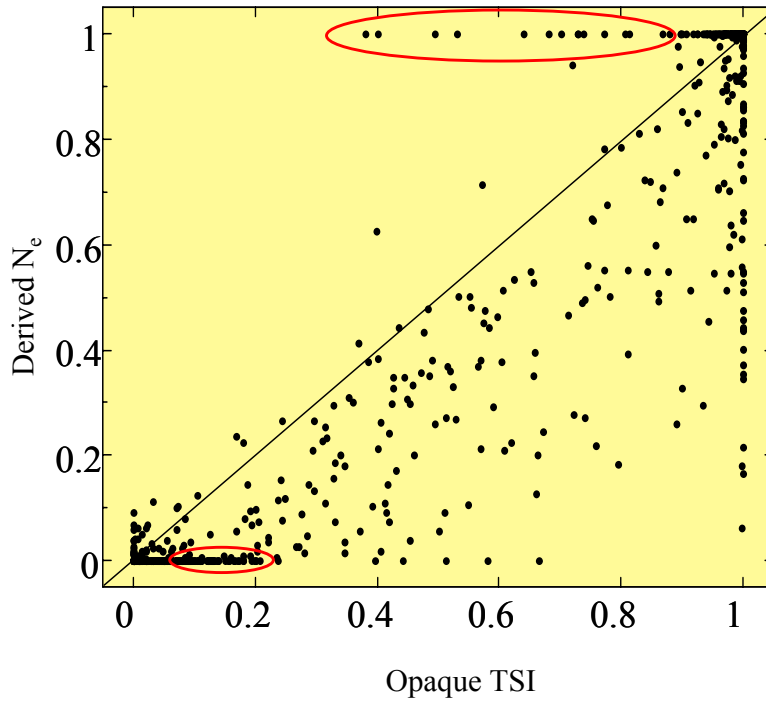


**Figure 1**.  Clouds with Zb < 4km and clear skies
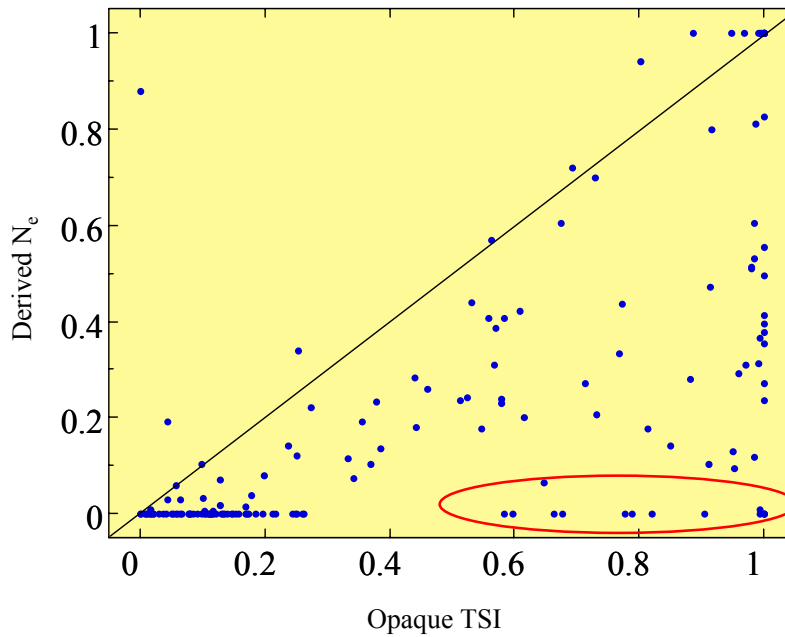


**Figure 2**.  Clouds with 4km ≤ Zb < 8km

Figure 3 is a scatter plot of the opaque TSI cloud amount and the derived $N_e$ for times where the $Z_b$ was greater than 8 km. This clearly shows the problem with detecting higher clouds using longwave instruments. The circled points show large amounts of cloud that are not detected with the derived $N_e$.
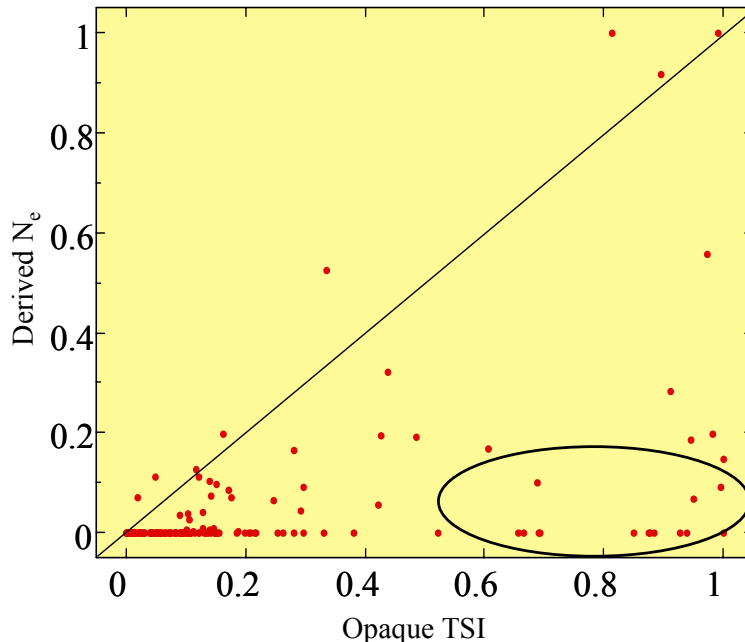


**Figure 3**.  Clouds with Zb $\geq$ 8km

## Summary and Conclusions

The effective cloud fraction (Ne) was compared with the hemispherical cloud amount for opaque clouds measured by the TSI. In all but a few cases, Ne was lower the TSI opaque cloud amount. The Ne showed limited agreement with the TSI for clouds below 4 km. The agreement between Ne and TSI decreased for middle and high clouds and as the number of cloud layers increased.

Since the longwave emission from middle and high clouds is significantly less than from low clouds, the downwelling radiance in the window region ($I_w$) may not be large enough to exceed the cloudiness threshold. This can make high clouds undetectable, as in Figure 3.

## Acknowledgments

## Corresponding Author

Dr. Ezra Takara, etakara@huey.met.fsu.edu, (850) 644-3340

# References

Han, D. and R. G. Ellingson, 1999: Cumulus cloud parameterizations for longwave radiation calculations. *J. Atmos. Sci.*, **56**, 837-851.